PCCP

Local silico-aluminophosphate interfaces within phosphated H-ZSM-5 zeolites†

Hendrik E. van der Bij and Bert M. Weckhuysen*

In order to elucidate phosphorus–zeolite H-ZSM-5 interactions, a variety of phosphorus-modified zeolite H-ZSM-5 materials were studied in a multi-spectroscopic manner. By deploying single pulse ^{27}Al, ^{31}P MAS NMR, 2D heteronuclear ^{27}Al–^{31}P correlation (HETCOR), ^{27}Al MQ MAS NMR spectroscopy, TPD of pyridine monitored by FT-IR spectroscopy, and Scanning Transmission X-ray Microscopy (STXM) the interplay and influence of acidity, thermal treatment and phosphorus on the structure and acidity of H-ZSM-5 were established. It was found that while acid treatment did not affect the zeolite structure, thermal treatment leads to the breaking of Si–OH–Al bonds, a decrease in the strong acid site number and the formation of terminal Al–OH groups. No extra-framework aluminium species was observed. Phosphorus precursors interact with the zeolitic framework through hydrogen bonds and physical coordination, as phosphorus species can be simply washed out with hot water. After phosphatation and thermal treatment two effects occur simultaneously, namely (i) phosphorus species transform into water insoluble condensed poly-phosphoric acid and (ii) phosphoric acid binds irreversibly to the terminal Al–OH groups of partially dislodged four-coordinated framework aluminium, forming local silico-aluminophosphate interfaces. These interfaces are potentially the promoters of hydrothermal stability in phosphated zeolite H-ZSM-5.

1. Introduction

One of the most promising alternative routes for the production of fuels and chemicals from fossil resources developed in the past few decades is the methanol-to-hydrocarbons (MTH) process. In this process methanol is selectively converted over a zeolite-based catalyst material into light olefins, paraffins as well as aromatics.[1,2] Methanol is produced from synthesis gas (CO/H$_2$), which in turn can be readily manufactured from all major hydrocarbon feedstocks, from natural gas to coal and biomass.[3] Recent increasing demands for light olefins and especially propylene have made the methanol-to-olefins (MTO) process the most commercially desirable member of the MTH catalyst family. The microporous solid acids H-SAPO-34 and H-ZSM-5 are the major players in the MTO process.[4] Whereas H-SAPO-34 shows a high selectivity towards ethylene and propylene, H-ZSM-5 shows a broader distribution of species, including aromatics and paraffins. However, improved olefin and especially propylene selectivity can be achieved using highly siliceous H-ZSM-5.[5,6] The selectivity towards propylene is increased even more with the introduction of phosphorus.[6–10] Usually, the improved selectivity

towards propylene is attributed to the decrease in the acid site strength that is so often observed in phosphated H-ZSM-5, although steric factors have also been suggested to be responsible.[6–12]

Even though there is still some debate on the effect of acid site strength on the MTO product distribution, the promoting effect of phosphorus on the hydrothermal stability of H-ZSM-5 is undisputed.[4,9,13–25] Zeolite H-ZSM-5 catalysts that contain phosphorus are more stable under hydrothermal conditions *i.e.* they retain more framework aluminium species and strong acid sites than their non-phosphated counterparts. Since the MTO process is performed at high temperatures and water is formed during methylation reactions, an improvement of hydrothermal stability is preferred. However, while the finding that improved propylene selectivity and hydrothermal stability are beneficial needs no further explanation, it is not known how these effects arise, as the exact nature of phosphorus–zeolite interactions is not yet understood. Not surprisingly, many models for possible interactions have been discussed over the years, where the main division of opinion lies between the question whether permanent phosphorus–framework interaction exists or not.[14,17,19,26–30,42]

In the case of permanent phosphorus–framework interaction the most intuitive explanation would be the incorporation of phosphorus into the zeolitic framework. However, the Si–O–P bonds that are required for such a substitution have never been found in either phosphorus/H-ZSM-5 or SAPO materials and theoretical work has pointed to the unlikeliness of such bonds.[14,15,17,20,29–32] Other possibilities of phosphorus–framework interaction have

Inorganic Chemistry and Catalysis, Utrecht University, Universiteitsweg 99, 3584 CG, Utrecht, The Netherlands. E-mail: b.m.weckhuysen@uu.nl; Fax: +31 30-251-1027

been suggested to arise from protonation of phosphoric acid by zeolitic bridging hydroxyl groups, stabilising the nearest neighbouring aluminium atom.[17] However, due to the low aluminium content generally found in H-ZSM-5, Al–O–Si–O–Al sites are quite rare and theoretical studies excluded the possibility of H_3PO_4 protonation.[30] The most promising proposal for framework Al–O–P bonds to date was one which included partially dislodged framework aluminium species.[15,29] Zhuang *et al.* and Damodaran and co-workers suggested that a hydrothermal treatment leads to the formation of partially dislodged aluminium, which reacts with phosphorus to form framework Al–O–P bonds.[15,29] Three types of Al–O–P bonds were distinguished using J-coupling ^{27}Al–^{31}P CP NMR, attributed to four-, five-, and six-coordinated Al–O–P species.[29]

Haw and co-workers suggested that phosphorus interacts with framework aluminium through hydrogen bonds.[9] This was supported by an early paper of Lischke *et al.* in which the reversible character of the phosphorus framework interaction was described, as phosphorus could be eluted using a hot water washing step. After a hydrothermal treatment phosphorus could not be washed out, which was attributed to the formation of insoluble extra-framework $AlPO_4$ species. Permanent phosphorus–framework interaction was suggested not to exist.[14] Caro and co-workers also proposed that phosphorus only interacted with extra-framework aluminium and that dealumination leads to a decrease in acid sites.[42]

These disagreements on zeolite–phosphorus interaction have led to much confusion with regard to the interpretation of data and spectra, as different authors attribute similar peaks to different species, *e.g.* in ^{27}Al MAS NMR and especially ^{31}P MAS NMR.[14,17,18,42] Another complicating factor is the synthesis conditions used during phosphatation, which vary for different studies. There are three parameters that can affect the structure of the zeolite material, namely (i) acidity coming from the acidic precursor H_3PO_4, which is often used, (ii) thermal treatment that is customarily performed after phosphorus introduction, and (iii) the actual presence of phosphorus species. Especially the effect of thermal treatment has never been investigated in detail, as it is nearly always performed after phosphorus introduction directly. Thermal treatment will have a strong effect on the state and number of framework aluminium sites and phosphorus species. In order to observe the sole effect of phosphorus on the zeolitic framework, it is important to study the phosphorus zeolite interactions before thermal treatment.

In this work we aim to provide a better understanding of the physicochemical processes that take place during phosphatation and obtain qualitative insight into phosphorus–zeolite interactions. We believe these insights are essential for the production of tailor-made phosphorus-modified zeolite catalysts. A set of samples, representing different steps in the phosphatation process, was prepared of which an overview is presented in Scheme S1 (ESI†). These samples have been studied using a multi-pronged spectroscopic approach, consisting of Fourier transform infrared spectroscopy (FT-IR), single pulse ^{27}Al, ^{31}P MAS NMR, 2D heteronuclear ^{27}Al–^{31}P correlation (HETCOR), ^{27}Al MQ MAS NMR spectroscopy, temperature programmed desorption (TPD) of

pyridine, as monitored with FT-IR, and scanning transmission X-ray microscopy (STXM). Using this combination of characterization techniques we have elucidated many physicochemical phenomena, *i.e.* the state, location and interaction of aluminium and phosphorus species, the number, type and strength of acid sites and the effects of the phosphate precursor, acid- and thermal treatment. Spectroscopic signatures for surface and bulk species will be presented to facilitate interpretation of past and future results. Finally, a synthesis route is proposed to obtain local silico-aluminophosphate (SAPO) interfaces within H-ZSM-5 materials, the potential promoters of hydrothermal stability.

2. Experimental section

2.1 Sample preparation

Commercially available Zeolyst CBV 2314 NH_4-ZSM-5 (Si/Al ratio = 11.5) was calcined in flowing dry air at 550 °C for 6 h. The obtained H-ZSM-5 material will be further referred to as [Z]. From the parent sample [Z] all other samples have been made. An overview of sample preparation can be found in the ESI,† S1. Sample NA[Z] was prepared by suspending 1.2 g of [Z] in a 200 ml aqueous solution of nitric acid (pH = 2.7) and 200 ml of hot water (70 °C), where it was stirred for 2 h. Afterwards the sample was retrieved by filtration and dried at 150 °C. Phosphatation was performed as described by Xue *et al.*[41] Sample PA[Z] was prepared by suspending 2.4 g of [Z] in an aqueous solution of an appropriate amount of H_3PO_4 in 200 ml of H_2O (P/Al ratio = 0.5, pH = 2.7), where it was stirred for 2 h. Afterwards, the solvent was removed by rotary evaporation. Subsequently, the sample was dried overnight at 150 °C. Sample PA[Z]e was prepared by suspending 0.6 g of sample PA[Z] in 200 ml of hot water (70 °C), where it was stirred for 2 h and subsequently filtered. PB[Z] was prepared by suspending 2.4 g of [Z] in an aqueous solution of an appropriate amount of $(NH_4)_2HPO_4$ in 200 ml of H_2O (P/Al ratio = 0.5, pH = 7.8), where it was stirred for 2 h. Afterwards, the solvent was removed by rotary evaporation. Subsequently, the sample was dried overnight at 150 °C. Sample PB[Z]e was prepared by suspending 0.6 g of sample PB[Z] in 200 ml of hot water (70 °C), where it was stirred for 2 h. Afterwards, the sample was retrieved by filtration and dried at 150 °C. Samples [Z]TT, NA[Z]TT, PA[Z]TT, and PB[Z]TT were prepared by calcination of sample [Z], NA[Z], PA[Z] and PB[Z] respectively in static air at 600 °C, for 5 h. Samples PA[Z]TTe, and PB[Z]TTe were prepared by suspending 0.6 g of sample PA[Z]TT and PB[Z]TT respectively in 200 ml of hot water (70 °C), where they were stirred for 2 h and then filtered.

Sample [Z]TT was resynthesised using identical conditions. 0.6 g of sample [Z]TT remade was suspended in a 200 ml aqueous solution of 0.06 M HNO_3 (pH < 0.89) where it was stirred overnight at 70 °C and subsequently filtered and dried. This acid leached sample is deemed [Z]TT A.L. Next, 1.2 g of sample [Z]TT remade was phosphated with H_3PO_4 using identical conditions as sample PA[Z]; this sample is deemed [Z]TT PA. Sample [Z]TT PA e was prepared starting from [Z]TT PA and applying an identical procedure as for sample PA[Z]e. Phosphorus loadings were determined by ICP analysis.

This journal is © the Owner Societies 2014

Phys. Chem. Chem. Phys., 2014, **16**, 9892–9903 | 9893

2.2   Solid-state nuclear magnetic resonance (NMR)

With the exception of samples [Z]TT remade, [Z]TT A.L., [Z]TT PA, [Z]TT PA e, and [Z]TT PA all MAS NMR experiments were performed at 18.8 T on a Bruker Avance 800 MHz spectrometer using a 3.2 mm HX low gamma MAS probe at room temperature. The MAS rate was 20 kHz for all experiments. The ^{27}Al NMR spectra were obtained using a pulse length of 1 μs, 1000 scans and a recycling delay of 2 s. The ^{27}Al 3Q-MAS were performed using a three pulse sequence. The spectra were obtained using 540 scans and a recycling delay of 1 s. The ^{31}P spectra were obtained using a pulse length of 1.8 μs, 64 scans and with a recycle delay of 60 s. The ^{27}Al–^{31}P CP experiments were acquired with 1600 scans, a recycle delay of 1 s, and with a contact time of 8000 μs. The chemical shifts of ^{27}Al, and ^{31}P were externally referenced to 1 M Al(NO$_3$)$_3$(aq), and 85% H$_3$PO$_4$(aq), respectively. All curve fittings were performed using the Dmfit software.[58]

The NMR experiments for the samples [Z]TT remade, [Z]TT A.L., [Z]TT PA, [Z]TT PA e, and [Z]TT PA were performed at 11.7 T on a Bruker Avance III 500 MHz spectrometer using a 4 mm MAS probe at room temperature. The MAS rate was 15 kHz for all experiments. The ^{27}Al NMR spectra were obtained using π/12 pulses, 1000 scans and a recycling delay of 0.5 s at a rf-field of 94 kHz. The ^{31}P spectra were obtained using a pulse length of 1.8 μs, 64 scans and with a recycle delay of 60 s. The chemical shifts of ^{27}Al, and ^{31}P were externally referenced to 1 M Al(NO$_3$)$_{3(aq)}$, and 85% H$_3$PO$_{4(aq)}$, respectively.

2.3   Scanning transmission X-ray microscopy (STXM)

STXM experiments were performed at the Canadian Light Source Beamline 10ID-1. Samples were dispersed in H$_2$O and a droplet was placed on a silicon nitride window. After drying in air the sample was placed in the STXM chamber, which was subsequently evacuated to 10^{-1} mbar. A polarized X-ray beam was obtained using a 2 m long, 76 mm period Apple II undulator. The X-ray beam was focused to 60 nm on the sample plane using a Fresnel zone plate (ZP). The beam from the ZP passed through a molybdenum-based order-sorting aperture (OSA), with a 50 μm pinhole. The OSA allowed only first-order ZP diffracted light to pass. Spectral image sequences (stacks) are measured by recording images over a range of photon energies. After aligning the image sequence, spectra of the whole or a subregion were extracted for comparison. All STXM data analysis was performed using aXis2000.

2.4   Fourier transform-infrared spectroscopy (FT-IR)

FT-IR measurements were performed on self-supporting zeolite wafers. 15 mg of the sample was pressed with 3 tons for 10 s into a thin disk. The sample was evacuated to 10^{-2} bar and heated at 7 °C min^{-1} to 600 °C and immediately cooled in steps of 25 K to 50 °C taking a spectrum at every interval. Pyridine was introduced in the vapour phase for 15 min and physisorbed pyridine was removed by outgassing at 50 °C and 10^{-2} bar for 30 min. TPD was performed by increasing the temperature in steps of 25 °C to 600 °C. For each step IR spectra were taken using a Perkin-Elmer FT-IR instrument with an optical resolution of 4 cm^{-1} and 12 accumulations with wavenumbers

ranging from 4000 cm^{-1} to 1000 cm^{-1}. Spectra were baseline corrected and normalized using the bands corresponding to zeolitic framework vibrations found at 1967 cm^{-1}, 1873 cm^{-1}, and 1637 cm^{-1}. To construct the pyridine TPD profiles, the normalized areas of the 1540 cm^{-1} peak were calculated from $T = 200$ °C to 600 °C. See Fig. S9 (ESI†) for the evolution of 1540 cm^{-1} bands with time. All values were a percentage relative to the area of the 1540 cm^{-1} band for sample [Z] at $T = 200$ °C.

3. Results

3.1   Effect of thermal and acid treatment

The zeolite H-ZSM-5 material under investigation has an ordered crystalline structure, which is confirmed by the data presented in Fig. 1. The ^{27}Al MAS NMR spectra show an intense and sharp signal at 54 ppm, which stems from Al atoms located at four-coordinated T-atom positions in the framework (TFAl species).[33] The O–H stretch vibrations of charge compensating protons that are found at these positions can be observed in the FT-IR spectra at around 3605 cm^{-1}.[34] Another resonance signal in the ^{27}Al MAS NMR spectra is found at 0 ppm, which is known to originate from octahedral framework Al (OFAl).[35,36] Three other vibrational bands, located at 3721 cm^{-1}, 3742 cm^{-1}, and 3780 cm^{-1}, can be found in the FT-IR spectra. These bands correspond to internal silanol groups, external silanol groups and external Al–OH groups, respectively.[34] The FT-IR spectrum of adsorbed pyridine, presented in Fig. S1 (ESI†), indicates that the sample contains both Brønsted acid sites and Lewis acid sites. Fig. 2a shows that pyridine desorption reaches a maximum at around 525 °C. The corresponding sites to this release are typically attributed to the Brønsted acid sites stemming from TFAl species.[37]

The effect of acid treatment on the zeolite structure is minimal. After treating sample [Z] in an aqueous nitric acid solution (pH = 2.7), we obtain sample NA[Z]. As shown in Fig. 1c and d, no changes in the ^{27}Al MAS NMR and FT-IR spectra are observed. Acid leaching of TFAl and OFAl is therefore unlikely, which is expected at a pH of 3.[38] Unexpectedly, the acidity profile of acid-treated NA[Z] changes. There is a loss
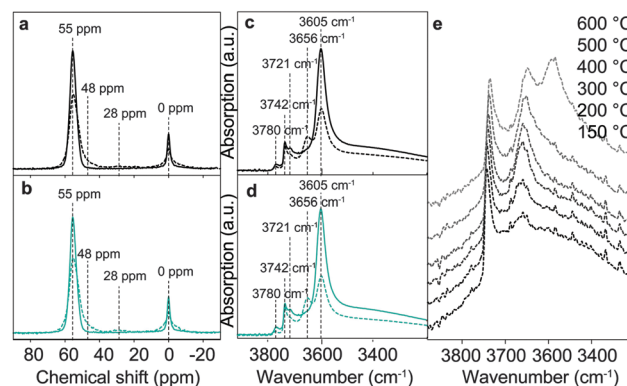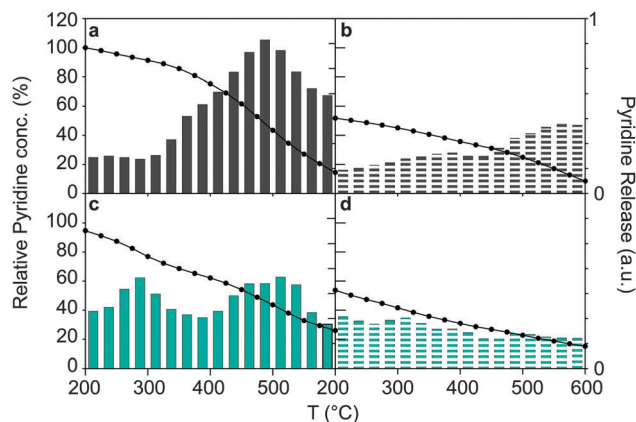

Fig. 1   (a and c) ^{27}Al MAS NMR spectra and (b and d) FT-IR spectra, highlighting the OH region of the following samples: — = [Z], - - - = [Z]TT, ▬ = NA[Z], and ---- = NA[Z]TT. (e) FT-IR OH-stretch spectra of sample [Z]TT during pyridine temperature programmed desorption.

Fig. 2 Profiles obtained during the temperature programmed desorption of adsorbed pyridine on different samples. The left y-axis shows a plotted line, which is the pyridine concentration relative to sample [Z] at 200 °C. The right y-axis shows the release of pyridine in between two temperature points as bars. The units are arbitrary but are normalized for each sample. (a) ■ = [Z], (b) ☰ = [Z]TT, (c) ■ = NA[Z], and (d) ☷ = NA[Z]TT.

Fig. 3 (a and b) ^{27}Al MAS NMR spectra and (c and d) FT-IR spectra, highlighting the OH-stretch region, and (e and f) ^{31}P MAS NMR spectra of the following samples: — = PA[Z], — = PA[Z]e, — = PB[Z], and — = PB[Z]e.

of strong acid sites and a slight increase in the number of weak acid sites.

After thermal treatment, both [Z]TT and NA[Z]TT experience a decrease in the number of TFAl sites, as shown in Fig. 1a and c. The decrease in the number of TFAl sites leads to a loss of the number of Si–OH–Al groups and a decrease in the number of Brønsted acid sites of approximately 45%. This is presented in Fig. 1b, d and 2; Table S1 (ESI†). A good correlation was found between the relative decrease in the number of TFAl species and the number of SiOHAl groups (Fig. S2, ESI†).

Simultaneously, a new type of distorted framework Al (TFAl$_{dis}$) is formed in samples [Z]TT and NA[Z]TT. This type of site can be seen using the ^{27}Al NMR technique as a distorted signal coming from TFAl located at 48 ppm and with the FT-IR technique as a vibrational band located at 3656 cm^{-1}. ^{27}Al MQ MAS NMR of sample [Z]TT is provided in the ESI† (Fig. S4), where it can be seen that the resonance has a different isotropic shift than the TFAl resonance, indicating a different kind of species. This resonance has a higher quadrupolar coupling than TFAl, representative of an asymmetrical environment. The acidic character of TFAl$_{dis}$ can be observed in Fig. 1e.

^{27}Al MAS NMR also shows a broadening of the resonance at 0 ppm indicating a decrease in crystallinity and the formation of a broad resonance at 28 ppm, which is often attributed to the presence of Al(v) species.[39] Interestingly, as can be seen in Fig. 2b and d, sample [Z]TT contains more strong acid sites, while sample NA[Z]TT has more weak acid sites. This follows from the pyridine Temperature Programmed Desorption (TPD) profiles of their respective parent materials.

3.2 Effect of phosphorus

After the introduction of phosphoric acid (PA) and ammonium hydrogen phosphate (PB) samples PA[Z] and PB[Z] are obtained. When H$_3$PO$_4$ is used as a precursor one can observe a decrease of about 30% in the number of TFAl species and SiOHAl groups, as
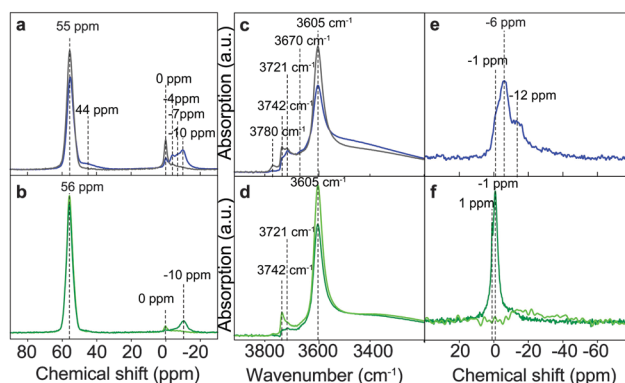
shown in Fig. 3; Fig. S2 and Table S1 (ESI†). Fig. 3b shows there is a decrease in the number of external silanol groups and external aluminol groups as well as the formation of a small band at 3670 cm^{-1} and a new broad band between 3520 and 3200 cm^{-1}. The latter two vibrational bands can be attributed to respectively P–OH groups and bridging hydroxyl groups interacting with oxygen.[40,41] All these effects can be observed in the spectra of a similar sample in the work of Lischke and co-workers.[14] Unfortunately, the authors did not mention nor comment on these spectral changes.

Four new resonances appear in the ^{27}Al MAS NMR spectra of sample PA[Z], seen in Fig. 3a. Fig. 4 shows the ^{27}Al MQ MAS NMR spectrum of sample PA[Z], which provides more evidence for the presence of these new species. The isotropic shift of resonance 3 is similar to the resonance attributed to TFAl. This indicates that these species are TFAl atoms with a larger quadrupolar coupling due to a highly distorted electronic environment. The three new six-coordinated aluminium species corresponding to signals 4, 5, and 6 lie along the anisotropic axis and are in a more symmetric environment. The ratio between the total number of Al(iv) species and Al(vi) species decreases, as shown in Table S4 (ESI†), which would indicate that Al(vi) species are formed at the cost of Al(iv) species.

^{27}Al–^{31}P HETCOR NMR spectra in Fig. 4 reveal that all the new aluminium species are in close proximity to phosphorus. The phosphorus species are dominantly found at −6 ppm, which can be attributed to pyrophosphates or terminal phosphate groups in polyphosphate chains.[42] The signal at −12 ppm is often attributed to middle chain phosphate groups.[42] The strongest Al–P interactions through space are found for the −15 ppm signal. Resonance 5 interacts with a variety of ^{31}P resonances.

The formation of new NMR resonances is accompanied with changes in both the number and strength of the acid sites (Fig. 5). As reported before, there is a decrease in the number of strong acid sites and an increase in the number of weak acid sites, giving rise to a weaker average site strength distribution.[14] In order to check the reversibility of the phosphorus interaction, samples were washed with hot water. Table S5 (ESI†) shows that after washing 75% of the P is removed and it is apparent from
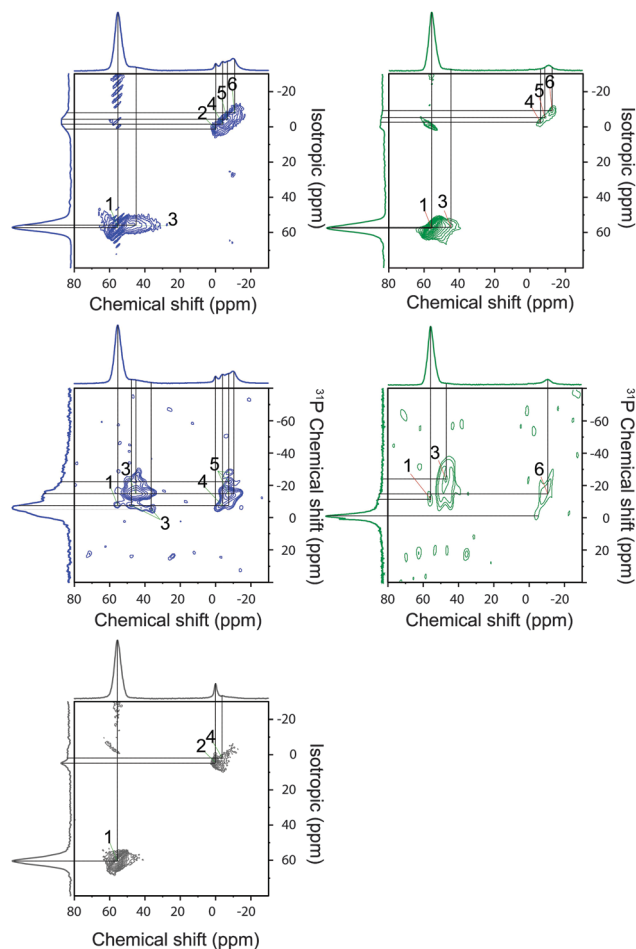
This journal is © the Owner Societies 2014

Phys. Chem. Chem. Phys., 2014, **16**, 9892–9903 | 9895

Fig. 4 ^{27}Al MQ MAS NMR and ^{27}Al–^{31}P CP HETCOR NMR spectra of the following samples: — = PA[Z], — = PA[Z]e, and — = PB[Z].
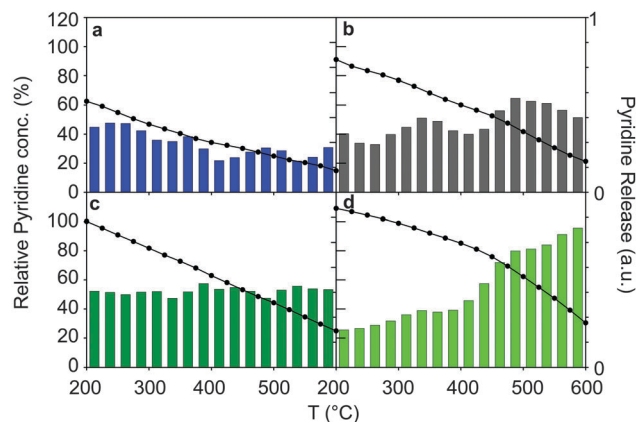

Fig. 5 Profiles obtained during the temperature programmed desorption of adsorbed pyridine on different samples. The left *y*-axis shows a plotted line, which is the pyridine concentration relative to sample [Z] at 200 °C. The right *y*-axis shows the release of pyridine in between two temperature points in bars. The units are arbitrary but are normalized for each sample: (a–d) samples ■ = PA[Z], ■ = PA[Z]e, ■ = PB[Z], and ■ = PB[Z]e.

Fig. 1 and 3 that the interaction of phosphorus is fully reversible as the ^{27}Al NMR and FT-IR spectra of sample PA[Z]e are similar to the parent material [Z]. When phosphorus is eluted, the pyridine desorption profile resembles that of the acid washed sample NA[Z].

When ammonium hydrogen phosphate is used as a precursor, the absorption intensity of the SiOHAl band does not decrease as can be seen in Fig. 3d. The intensity of the 55 ppm peak, corresponding to TFAl species, is larger than for the parent [Z] sample. Furthermore, Fig. S5 (ESI†) shows that the spinning side bands of the 55 ppm resonance increase in intensity, indicating a more symmetric environment for the TFAl species in sample PB[Z]. In agreement with these findings are the limited Al–P interactions, as observed with the ^{27}Al MQ MAS and ^{27}Al–^{31}P HETCOR NMR techniques shown in Fig. 4.

The types of phosphorus–framework interactions are similar to that of PA[Z], although minor in intensity as shown in Fig. 4. The ^{31}P NMR spectra of PB[Z] in Fig. 3f reveal that most of the phosphorus is represented by the 0 ppm resonances, corresponding to ammonium hydrogen phosphate.[43] ^{31}P resonances of sample PB[Z] at −12 ppm interact with the newly formed Al species at −10 ppm, as depicted in Fig. 4. There is a strong

decrease in the number of external Si–OH groups and internal Si–OH groups as can be seen in Fig. 3d. The acid site strength is heterogeneous in nature, with an equal and continuous distribution of weak and strong acid sites as shown in Fig. 5c.

After elution the number of TFAl species increases even further and a comparison with the parent sample [Z] is presented in Fig. S6 (ESI†). The treatment with ammonium hydrogen phosphate followed by washing, leads to a decrease in the 0 ppm resonance (OFAl species), an increase in the 55 ppm resonance (TFAl species).

The intensity for TFAl species is 10% higher than parent sample [Z], and there is a corresponding increase in the number of SiOHAl species, as follows from Fig. S2 and Table S1 (ESI†). There is a strong decrease in the number of internal Si–OH and Al–OH species, though the band for external Si–OH species reappears, as seen in Fig. 3d.

The total acid site number and average acid site strength increase as sample PB[Z]e is able to retain more pyridine at higher temperatures as compared to parent sample [Z], as shown in Fig. 5d.

3.3 Effect of thermal treatment on phosphated samples

Although the choice of phosphate precursor leads to a difference in structure and acidity of the H-ZSM-5 material, a subsequent thermal treatment nullifies these differences. As can be witnessed from the aluminium K-edge, ^{27}Al, ^{31}P (MQ) MAS NMR, ^{27}Al–^{31}P CP HETCOR, FT-IR spectra and the pyridine TPD profiles in Fig. 6–9, the samples PA[Z]TT and PB[Z]TT are close to identical. In Fig. 6 and Table S1 (ESI†) it can be seen that the thermal treatment of PA[Z] and PB[Z] leads to a 80% decrease in the number of TFAl species and SiOHAl groups. As mentioned for samples NA[Z]TT and [Z]TT the decrease caused by the thermal treatment was 45%, so 35% of the total decrease can be attributed to the presence of phosphorus.

The ^{27}Al MQ MAS NMR spectra in Fig. 7 show that resonances 3, 4, 5 and 6 have increased in intensity and broadened, indicating a larger distribution of these species in samples PA[Z]TT and PB[Z]TT. There is a shoulder on the isotropic axis
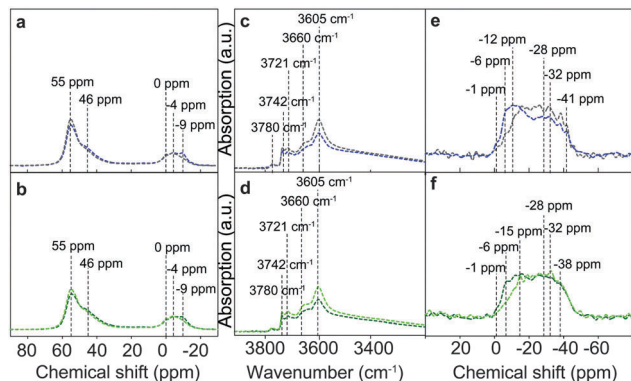
Fig. 6 (a and b) ^{27}Al MAS NMR, (c and d) FT-IR OH-stretch region spectra, and (e and f) ^{31}P MAS NMR of samples ---- = PA[Z]TT, ---- = PA[Z]TTe, ---- = PB[Z]TT, and ---- = PB[Z]TTe.

at 57 ppm, indicating a new type of species, similar to the one found for sample [Z]TT. ^{31}P MAS NMR spectra presented in Fig. 6e and f, reveal that thermal treatment leads to a wide variety of phosphates, of which the majority is in close vicinity to aluminium. There are many P–Al correlations found, shown in Fig. 7 and phosphorus species with a resonance at −15 ppm
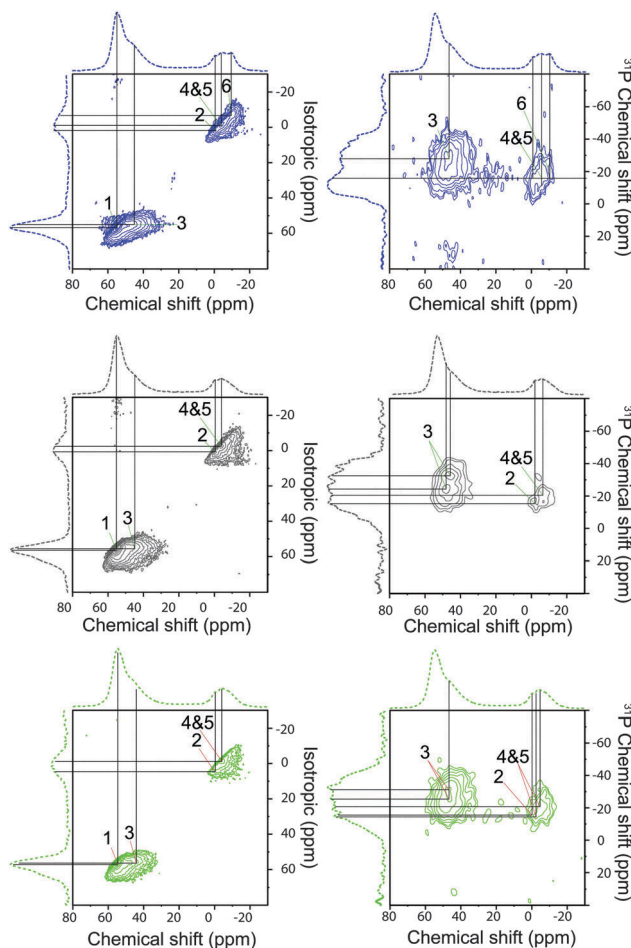

Fig. 7 ^{27}Al MQ MAS NMR and ^{27}Al–^{31}P CP HETCOR NMR for the samples: ---- = PA[Z]TT, ---- = PA[Z]TTe, and ---- = PB[Z]TTe.
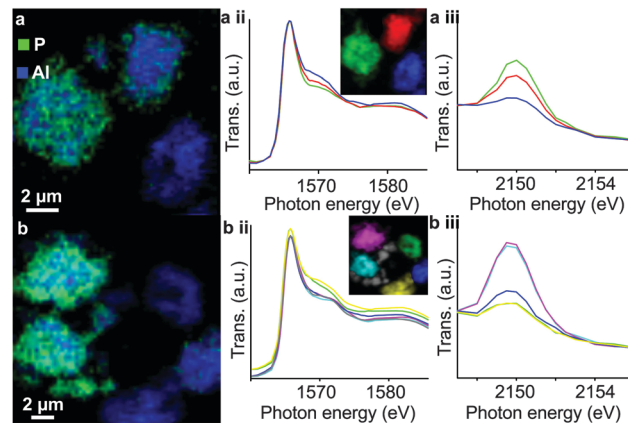

Fig. 8 Chemical maps of zeolite clusters, constructed from aluminium K-edge spectra and phosphorus K-edge spectra stacks, displaying samples PA[Z]TT (a) and PB[Z]TT (b). ■ = Al ■ = P resolution is 60 × 60 nm. (a, ii) and (b, ii) Aluminium K-edge XANES spectra, each spectra is colored according to the corresponding cluster in the inset. (a, iii) and (b, iii) Phosphorus K-edge XANES spectra, each spectra is colored according to the corresponding cluster in the inset.

interact with most of the OFAl species, while most of the TFAl$_{dis}$ species interact with phosphorus at a broad number of resonances centred at around −28 ppm. For sample PA[Z]TT there is an interaction between ^{31}P at −15 ppm and ^{27}Al at 26 ppm, which could correspond to Al(v) species.

The average acid strength distributions for samples PB[Z]TT and PA[Z]TT shift to weaker average acidities, as shown in Fig. 9a and c which is in accordance to literature.[7,12,14,17,18]

STXM data presented in Fig. 8 reveal both inter-, and intra-particle heterogeneities in the distribution of phosphorus. As recently reported by our group, there is a gradient in the phosphorus distribution, revealing a higher concentration of phosphorus closer to the external surface of the H-ZSM-5 particle.[60] Furthermore, the phosphorus-modification method leads to an inhomogeneous distribution of phosphorus between different clusters.

The aluminium K-edge XANES spectra of the parent sample presented in Fig. S7 (ESI†) resemble those recorded for zeolite H-ZSM-5, with a white-line at 1565 eV and two features at +5 eV and +10 eV from this position.[44,45] Clusters that do not contain high loadings of phosphorus have a broadened post-edge feature at around +5 eV in the aluminium K-edge XANES spectra, also seen for very mildly steamed zeolites, which are attributed to distorted Al species.[45] However, samples containing high phosphorus content have a sharply decreased post-edge feature, indicating a change in the neighbouring atoms of aluminium.

The latter finding indicates that with higher loadings of phosphorus, more phosphorus can penetrate into the zeolite, with more aluminium atoms being affected by the presence of phosphorus.

Washing results only in the elution of a fraction of phosphorus, with still 75% of the original phosphorus content remaining (Table S5, ESI†). This could be explained by the formation of water insoluble condensed poly-phosphoric acid that is formed after thermal treatment, as shown in Fig. S8 (ESI†). However, from Fig. 7 it becomes clear that the phosphorus that is in close vicinity to aluminium is not washed out.
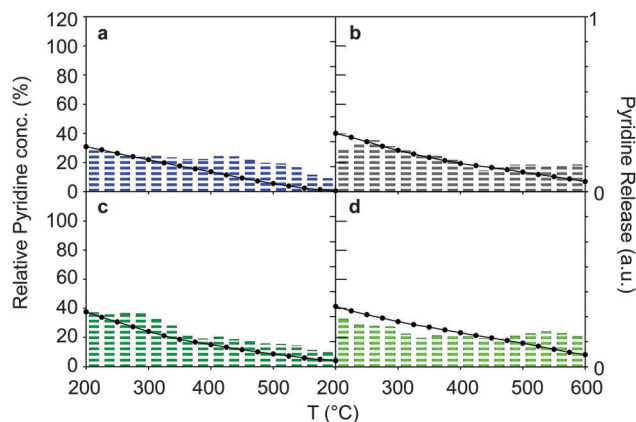
Fig. 9 Profiles of temperature programmed desorption (TPD) of adsorbed pyridine for the different samples under study. The left y-axis shows a plotted line, which is the pyridine concentration relative to sample [Z] at 200 °C. The right y-axis shows the release of pyridine in between two temperature points in bars. The units are arbitrary, but are normalized for each sample. (a–d) Samples: ■ = PA[Z]TT, ■ = PA[Z]TTe, ■ = PB[Z]TT, and ■ = PB[Z]TTe.

Fig. 10 (a and b) ^{27}Al MAS NMR spectra, (c and d) FT-IR spectra, highlighting the OH-stretch region, and (e) ^{31}P MAS NMR spectra of the following samples: ---- = [Z]TT remade, —— = [Z] TT A.L., —— = [Z]TT PA, and —— = [Z]TT PA e.

Fig. 6e and f show that the ^{31}P resonances at around −6 ppm to −12 ppm, which have no strong correlation with aluminium, are sharply decreased after washing.

Fig. 7 shows that for both samples PB[Z]TTe and PA[Z]TTe Al–P correlations disappear, including ^{27}Al resonance 6 with ^{31}P resonance at −15 ppm and ^{27}Al resonances at 20 ppm to 25 ppm with ^{31}P resonance at −19 ppm. After washing two types of phosphorus with resonances at −24 ppm and −32 ppm interact with aluminium in resonance 3. The two types of species stem from the same ^{27}Al NMR resonance, so it is more likely that these are two types of phosphorus interacting with one type of aluminium than *vice versa*. Phosphorus resonances at higher chemical shifts, *i.e.*, −19 ppm and −15 ppm, interact with the OFAl species. The washing results in a 20% increase in the number of TFAl species and SiOHAl sites (Table S1, ESI†). Unaffected TFAl species are not in close vicinity with phosphorus. Although the average acid site strength distribution does not change significantly, the number of protonated pyridinium ions increases by approximately 10% as shown in Fig. 9b and d.

3.4 Effect of thermal treatment preceding phosphatation

From the results described above it can be deduced that either, (i) Al–O–P bonds do not exist in hydrated samples and the only interactions between the two atoms are through space. Additionally, the formation of water insoluble phosphorus species after thermal treatment prevents phosphorus to be eluted, or (ii) TFAl$_{dis}$ species that are formed after thermal treatment react irreversibly with phosphates. This would lead to framework Al–O–P bonds and the formation of local silico-aluminophosphate (SAPO) interfaces. To test these two hypotheses sample [Z]TT has been resynthesised and subsequently phosphated.

First the sample was suspended in an aqueous HNO$_3$ solution to test if the TFAl$_{dis}$ species could be washed out and would therefore be extra-framework. As can be seen in Fig. 10a
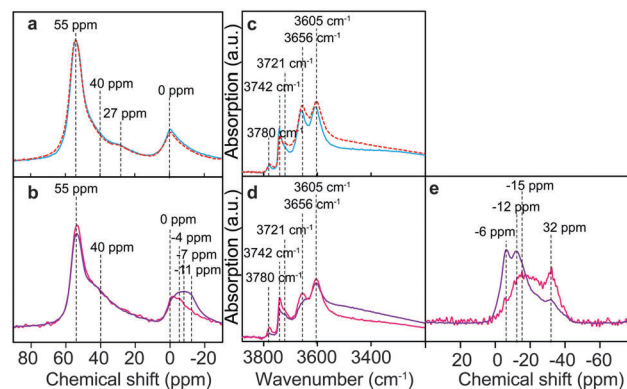
and c, this was not possible and the presence of EFAl species can therefore be excluded. After phosphatation of [Z]TT with H$_3$PO$_4$, both the ^{27}Al, ^{31}P MAS NMR and FT-IR spectra shown in Fig. 10b, d and e resemble sample PA[Z]TT.

Resonances 3, 4, 5, and 6 are present. There is a strong decrease in intensity for the band at 3650 cm^{-1} attributed to TFAl$_{dis}$ species. It is encouraging to see that the resonances at −32 ppm and −15 ppm are present, indicating that these species are not formed due to hydrothermal treatment after phosphatation.

After elution with hot water, it can be observed that the resonances 3, 4, and 5 remain, while only a fraction of the 3650 cm^{-1} band is retrieved. Although the remaining amount of phosphorus content of 40% is similar to that of PB[Z]e, the ^{31}P MAS NMR spectra are completely different and resemble that of the samples PB[Z]TTe and PA[Z]TTe. The resonance at around −32 ppm has remained, as do the broad resonances at around −23 ppm and −15 ppm. We can therefore attribute these resonances to the presence of phosphate species exclusively and irreversibly interacting with TFAl$_{dis}$ and OFAl$_{dis}$ species.

4. Discussion

By precisely following the different steps in the phosphorus post-modification process using an array of spectroscopic methods we have established the type of Al species present in H-ZSM-5 and the phosphorus interactions with these species. An overview of the species and their spectroscopic signatures is given in Table 1.

4.1 Formation of partially dislodged TFAl species

The parent zeolite H-ZSM-5 has an ordered crystalline structure comprising two types of framework aluminium. Namely tetrahedrally coordinated framework aluminium species (TFAl) and octahedrally coordinated framework aluminium species (OFAl), both are schematically drawn in Fig. 11a and b respectively. The latter is connected with three bonds to the framework and possesses an octahedral coordination in hydrated form

Table 1 Type of species found in phosphorus-modified H-ZSM-5 materials

Type of species	Description	Spectroscopic signature	Acid type
TFAl	Tetrahedrally coordinated framework Al and corresponding bridging hydroxyl groups	3604^a, 55^b $(1)^c$	Brønsted
OFAl	Octahedrally coordinated triple-bound framework Al physically coordinated to three H_2O molecules	Partial 3780^a, 0^b $(2)^c$	Lewis
TFAl$_{dis}$	Partially dislodged tetrahedrally coordinated double-bound framework Al with two hydroxyl groups	3656^a, 48 (and 28)^b	Brønsted
Si–OH ext	External Si–OH	3742^a	Brønsted
Si–OH int	Internal Si–OH located next to OFAl species	3721^a	Brønsted
TFAl + H_3PO_4 (a)	Bridging hydroxyl groups hydrogen bonded with H_3PO_4	$3500–3200^a$, 44^b $(3)^c$	Uncertain
TFAl + H_3PO_4 (b)	TFAl species adopting octahedral coordination by physical coordination with two H_3PO_4 or $(NH_4)_2HPO_4$ molecules	-10^b 6^c, -15^d	Uncertain
OFAl + H_3PO_4	Octahedrally coordinated triple-bound framework Al physically coordinated to x H_3PO_4 molecules and $3-x$ H_2O molecules. x = 1 or 2	-4, and -7^b $(4, 5)^c$, -15^d	Uncertain
TFAl$_{dis}$–O–P	Partially dislodged tetrahedrally coordinated double-bound framework Al bonded to one or two phosphate monodentate or bidentate species	-44^a, $(3)^b$, -24^d, -32^d	Uncertain

^{a} Wavenumber (cm^{-1}). ^{b} ^{27}Al chemical shift (ppm). ^{c} ^{27}Al MQ MAS resonance. ^{d} ^{31}P chemical shift (ppm).

with three framework oxygen atoms and three oxygen atoms in H_2O (OFAl).

In dehydrated form these OFAl species transform into threefold coordination with the three framework oxygen atoms, as can be seen in Fig. 11d.[46,47] As the samples have been dehydrated for FT-IR measurements no OH groups connected to these species can be seen in the spectra, except for external terminal Al–OH groups. Brønsted acidity comes from Si–OH–Al bridging hydroxyl groups at TFAl sites and the Lewis acidity comes from the dehydrated three-coordinated aluminium sites.[35,45]

The effect of acid treatment during phosphatation on the structure and acid site number of H-ZSM-5 is negligible. Still, it is found that acid treatment does shift the acid site strength distribution, as there is a decrease in the number of strong acid sites and an increase in the number of weaker acid sites. Thermal treatment, on the other hand, has an altering effect on the structure and acidity of H-ZSM-5. High temperatures and the small concentration of water in the air lead to partial dealumination. We use the word partial to describe the breaking of Si–O–Al bonds and the formation of partially dislodged aluminium species. Based on literature we attribute these species to tetrahedrally coordinated aluminium that is connected with only two bonds to the framework (TFAl$_{dis}$).[48] Two terminal Al–OH groups are formed and one proton compensates for the negative charge on the framework, as can be seen in Fig. 11c. The acidic bridging SiOHAl group of this species is responsible for the 3656 cm^{-1} FT-IR band.

Density Functional Theory (DFT) calculations performed by other groups predicted these species to form in early stages of dealumination.[49–51] It was suggested that in the hydrated form they can be penta-coordinated, with aluminium binding with one extra water molecule, which would explain the small amount of Al(v) species observed using ^{27}Al MAS NMR.[49] These species do still possess Brønsted acidity as they are able to protonate pyridine. Acid leaching does not remove these species, excluding that they are extra-framework.[48]

The decrease in the number of TFAl species leads to a decrease in the number of strong Brønsted acid sites with about 45%.
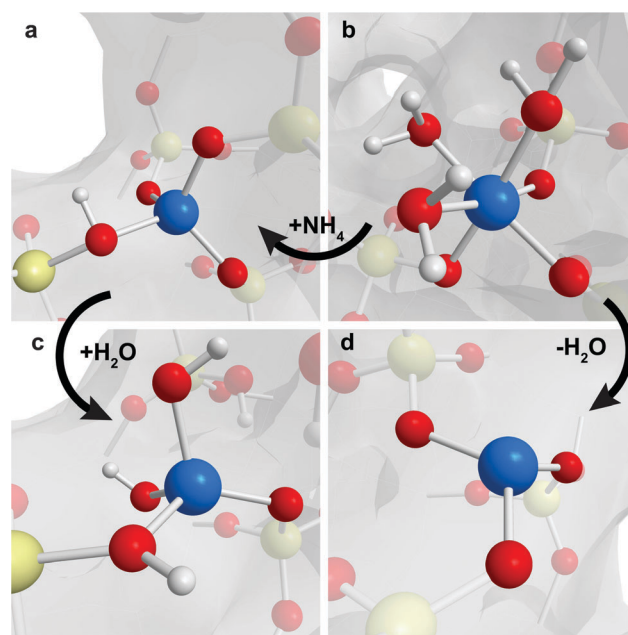

Fig. 11 Schematic representation of four different aluminium species found in the H-ZSM-5 framework, located at the straight and sinusoidal channel intersection. (a) Tetrahedrally coordinated framework aluminium (TFAl) forming a bridging hydroxyl group with neighboring Si. (b, d) Octahedrally coordinated framework aluminium (OFAl) interacting with three water molecules in hydrated form. In dehydrated form it forms three-coordinated aluminium. (c) Distorted tetrahedrally coordinated framework aluminium (TFAl$_{dis}$), only attached with one or two bonds to the zeolitic framework. Three protons compensate the negative charge on the $(SiO)_2AlO_2^{3-}$ unit. ▪ = Si, ▪ = Al, ▪ = O, ☐ = H.

4.2 Reversible phosphorus–framework interactions

Phosphatation with H_3PO_4 does not lead to a noticeable dealumination of the material, as H_3PO_4 can be easily removed from the zeolite by hot water washing, returning the zeolite to its former state. This indicates that the interaction of phosphorus with the zeolite is not through covalent bonds. However, there is an interaction of phosphorus with framework aluminium.

This journal is © the Owner Societies 2014

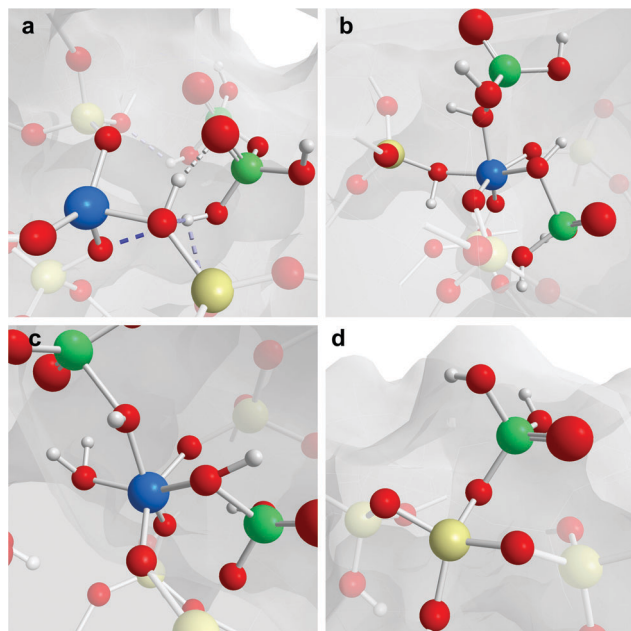Phys. Chem. Chem. Phys., 2014, **16**, 9892–9903 | **9899**

Fig. 12 Schematic representation of simplified reversible phosphorus–framework interactions (a) TFAl interacting with phosphoric acid through hydrogen bonds, (b) TFAl physically coordinated with two phosphoric acid molecules, adopting a six-coordination, (c) OFAl species physically coordinated by two phosphoric acid molecules and one water molecule, (d) the condensation reaction between silanol groups and phosphoric acid, induced by dehydration. ▢ = Si, ■ = Al, ■ = O, ▢ = H, ■ = P.

Phosphorus in close vicinity to TFAl has a distorting effect on its symmetric surrounding, as shown by ^{27}Al MQ MAS NMR. We would like to follow the suggestion of Haw and co-workers that these distortions arise from a hydrogen bond between the bridging hydroxyl group and a phosphate oxygen atom as is shown in Fig. 12a.[9] The appearance of the broad band in FT-IR between 3520 cm^{-1} and 3200 cm^{-1}, which indicates intramolecular bonds between framework protons and oxygen, supports this.[40]

Furthermore, OFAl species that can coordinate with three water molecules, appear to be able to coordinate with phosphorus as well. Since three new resonances are found for OFAl species, it is tempting to attribute these to $(SiO)_3Al(H_2O)_{3-x}(H_3PO_4)_x$ (x = 1, 2, or 3), which is depicted in Fig. 12c. However, the length of polyphosphoric chains that interact could also have an effect on the chemical shift. Especially resonance 5 is interacting with different types of phosphorus species. Finally, the fact that Al(IV)/Al(VI) ratios decrease significantly after H_3PO_4 introduction, indicate that TFAl species can also physically coordinate with phosphoric acid, adapting a reversible octahedral coordination, as has been suggested in the literature, where a ^{27}Al chemical shift and ^{31}P chemical shift at −10 ppm and −12 ppm were reported respectively.[14,59] This species is shown in Fig. 12b.

It is uncertain if phosphorus species that are close to aluminium actually affect the acidity of H-ZSM-5 in its hydrated form.

Nevertheless, the reversible decrease in the number of T–OH groups and bridging hydroxyl groups, as observed with FT-IR, indicates that phosphorus is interacting with these groups.

Furthermore, the reversible decrease of 30% of the Brønsted acid sites corresponds very well with the 30% decrease in TFAl species as can be seen in Fig. S2 (ESI†). The decrease in Si–OH–Al groups observed with FT-IR can be attributed to the hydrogen bonds that bridging hydroxyl groups form with nearby phosphorus, leading to a shift of the band from 3520 cm^{-1} to 3200 cm^{-1} and TFAl species that adopt six-fold coordination. The decrease in protonated pyridine molecules would then stem from steric hindrance caused by nearby phosphate species.

Although Si–O–P bonds formed by silanol with phosphorus interaction have been shown to be unstable under hydrous conditions, they have been found to be stable in a water-free environment.[52,53]

One should consider that FT-IR experiments, and for that matter many other characterization techniques to probe acid sites (including ^{1}H NMR), are performed in the absence of water. Therefore, dehydroxylation is promoted and consequently, although unstable, P–O–Si bonds can form, as proposed in Fig. 12d. This is observed as the P–O–H vibrations appear at 3670 cm^{-1}.

It is important to realize that the decrease in acid site number and strength does not necessarily require permanent phosphorus–framework interactions. After washing there is a redistribution of the acid site strength towards weaker average site strength. As this result is very similar to washing with a nitric acid solution with the same pH, we attribute the effect to an acid treatment.

4.3 Ammonium hydrogen phosphate as the precursor

Ammonium hydrogen phosphate does not interact as strongly with H-ZSM-5 as orthophosphoric acid. It is mostly present as ammonium hydrogen phosphate. The minimal interaction that is observed with aluminium is similar to orthophosphoric acid interaction, as shown using ^{27}Al MQ MAS NMR. However, the type of phosphorus species interacting is different. Since FT-IR spectroscopy does not show a decrease in the amount of SiOHAl species and only a decrease in the number of external Si–OH groups, we propose that the reason for minimized interaction is due to the location of ammonium hydrogen phosphate, which would be on the external zeolitic surface.

The fact that NH_4^+ acts as a counter cation for SiOHAl groups, leads to the repair of formerly broken Al–O–Si bonds and an increase in the amount of TFAl species. This effect has been described previously by Woolery and co-workers and was attributed to the healing of three-coordinated framework Al (OFAl) species to four-coordinated species under the influence of NH_4^+.[35,45] This effect has also been observed for zeolite Beta treated with K and Na cations.[54] The conversion of Lewis acid OFAl species into Brønsted acid TFAl species is followed by a decrease in the absorption intensity for coordinately bound pyridine (1454 cm^{-1}) and an increase in the absorption intensity for protonated pyridinium ions (1540 cm^{-1}).

This effect is especially clear when the ammonium hydrogen phosphate is washed out and an increase in the amount of TFAl species, SiOHAl groups and Brønsted acid sites, plus a decrease in the number of OFAl species and Lewis acid sites is observed. A decrease in the number of internal Si–OH groups indicates that these species are positioned next to three-coordinated

aluminium sites and share a previously broken oxygen bond. A decrease in the number of surface Al–OH groups indicates that these species can form TFAl species as well and are the only OFAl species that stay visible in FT-IR after dehydration. Following this reasoning and assuming that in sample PB[Z] all OFAl species are transformed into TFAl species, one can observe that for sample PB[Z] the only six-fold coordinated species is resonance 6. Consequently, this resonance is attributed to TFAl species reversibly adopting a octahedral coordination after coordinating with two diammonium hydrogenphosphate or phosphoric acid molecules.

4.4 Permanent phosphorus–framework interactions

Thermal treatment of PA[Z] and PB[Z] leads to two similar materials. There is an 80% decrease of TFAl species and SiOHAl groups. ^{27}Al MAS NMR resonances found for Al–P interaction are similar to those for PA[Z], but have a higher distortion and an increased intensity. The resonances of phosphorus shift to lower chemical shifts, which indicate a different type of interaction. The interaction of phosphorus with distorted framework aluminium seen as resonance 3 in ^{27}Al MQ MAS NMR is a broad resonance with a higher quadrupolar coupling than TFAl, not dissimilar to those found for the SAPO interfaces in SAPO materials, such as SAPO-34 and SAPO-11.[55] Furthermore, in the open literature reported J-coupling experiments have shown a direct Al–O–P bond for resonance 3 and the −32 ppm resonance observed in ^{31}P MAS NMR.[29] The change in the aluminium K-edge XANES post-edge feature for samples with high phosphorus loadings, indicates a change in neighbouring atoms.

Whether a thermal treatment follows or proceeds phosphorus introduction, the type of interactions found for ^{27}Al and ^{31}P MAS NMR are the same and washing with hot water does not remove all of these newly formed species.

4.5 Formation of local SAPO interfaces

Considering the results, we feel comfortable to propose a model for P–O–Al framework interaction, which elaborates on a previous model proposed by Zhuang et al. and Damodaran and co-workers.[15,29] Thermal treatment leads to the formation of TFAl$_{dis}$ species. Consequently, the free Al–OH groups can react with phosphoric acid to form bidentate $(SiO)_2Al(O_2P(OR)_2)$ or $(SiO)_2Al(O_2P_2O_2(OR)_3)$ species where R = H or (poly)phosphoric acid, giving rise to local SAPO interfaces. These species are presented in Fig. 13.

It was found that for the porous alumina surface Al–OH groups readily reacted with H_3PO_4 to form surface Al–O–P groups.[56] We need to stress that irreversible phosphorus interaction with Al–OH species does not occur for terminal triple-bound framework Al–OH groups observed using FT-IR, as these species react reversibly with phosphorus. ^{31}P MAS NMR indicates that at least two types of phosphorus species bind with TFAl$_{dis}$ species at −32 ppm and −24 ppm. The former has been ascribed to an aluminium-bound mono- or bidentate middle chain phosphate species.[29,57]

The latter at −24 ppm has been ascribed to either aluminium-bound middle chain phosphate species, extra-framework AlPO or condensed polyphosphates.[29,57] Since the formation of EFAl is excluded we would not expect the formation of extra-framework
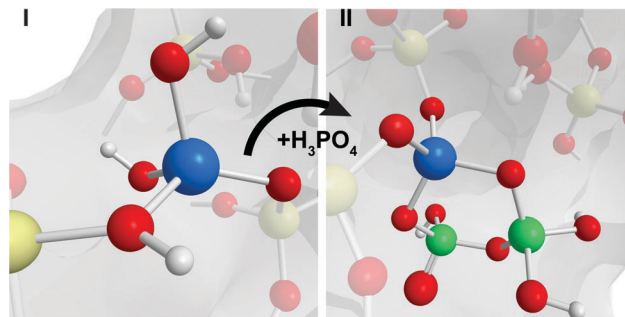

Fig. 13 Schematic representation of (a) TFAl$_{dis}$, (b) the proposed result of TFAl$_{dis}$ after reaction with phosphoric acid. ▢ = Si, ▢ = Al, ▢ = O, ▢ = H, ▢ = P.

AlPO species and condensed polyphosphates will only form after thermal treatment. Therefore we can only attribute the −24 ppm species to aluminium-bound middle chain phosphate species. As the ^{31}P MAS NMR spectra show quite a broad distribution, there are probably multiple Si–Al–O–P type phosphate species.

Whether the local SAPO interfaces form a new type of weak acid site, which has often been described in the literature, remains uncertain. It is clear that an acid treatment followed by a thermal treatment already leads to a decrease in the average acid site strength, while the aluminium connected with two SiO and one PO group will not require counter cations. Interestingly, it was reported that the formation of surface Al–O–PO(OH)$_3$ groups in porous alumina, was followed by a decrease in the number of strong acid sites and in the concomitant increase in the number of weak acid sites.[56] This phenomenon was attributed to the decrease in the number of Al–OH groups and the increase in the number of P–OH groups.

5. Conclusions

By modifying H-ZSM-5 using a phosphorus precursor, a large variety of aluminium and phosphorus species are formed. In this work several have been identified, leading to new insights into phosphorus–framework interactions and its effect on zeolite acidity. Most importantly, by impregnating H-ZSM-5 containing partially dislodged tetrahedrally coordinated framework aluminium (TFAl$_{dis}$) species using a phosphate precursor, it is possible to introduce local silico-aluminophosphate (SAPO) interfaces, proving that permanent phosphorus–framework interactions can exist.

The formation of TFAl$_{dis}$ species occurs during thermal treatment, when elevated temperatures and water present in the atmosphere hydrolyse two Si–O–Al bonds, giving rise to a distorted four coordinated acidic framework Al species. This TFAl$_{dis}$ species is connected with only two bonds to the framework. Two terminal Al–OH groups are formed and one proton compensates for the negative charge on the framework. When phosphorus is present it readily reacts with the Al–OH groups of the dislodged species, forming a framework–$(SiO)_2$–Al–$(PO)_2$ type species. Introducing the phosphate precursor before or after a thermal treatment leads to structurally similar materials, with the

exception of water insoluble condensed poly-phosphoric acid, which only forms during thermal treatment.

After thermal treatment of phosphated H-ZSM-5 materials there is, irrespective of the phosphate precursor, a strong decrease in the number of acid sites as well as a shift towards weaker average acid site strength. A large part of this decrease can be attributed to partial dealumination induced by thermal treatment. However, a significant other part is caused by the presence of phosphorus. Due to charge compensation it is unlikely that the local SAPO interfaces have a Brønsted acid site similar to microporous SAPO materials, such as H-SAPO-34 or H-SAPO-11. Possibly the terminal P–OH groups of the interfaces are responsible for the formation of weak acid sites.

If a thermal treatment is not performed, the interaction of the phosphate precursors is fully reversible. Phosphate precursors physically coordinate with, (i) octahedrally coordinated framework Al (OFAl) species and (ii) the tetrahedrally coordinated framework (TFAl), which adopts a six-fold coordination. Furthermore, the bridged hydroxyl protons found in TFAl species form an intra-molecular bond with nearby phosphate oxygen groups present in (poly)-phosphoric acid. These interactions lead to an observed reduction in the number of strong acid sites and an increase in the number of weak acid sites. After washing, the acid number and strength increase again. Therefore, it can be concluded that the observed decrease in acid site number and strength does not require permanent or stable phosphorus–framework interactions.

Performing a pre-thermal treatment before phosphorus introduction, followed by hot water washing, provides a material where phosphorus is almost exclusively situated in local SAPO interfaces. With the nature of phosphorus–framework interactions being elucidated, it is possible to investigate if these species are responsible for the improved hydrothermal stability found in phosphated H-ZSM-5.

Acknowledgements

Notes and references

1 F. J. Keil, *Microporous Mesoporous Mater.*, 1999, **29**, 49–66.
2 M. Stöcker, *Microporous Mesoporous Mater.*, 1999, **29**, 3–48.
3 K. C. Waugh, *Catal. Today*, 1992, **15**, 51–75.
4 U. Olsbye, S. Svelle, M. Bjørgen, P. Beato, T. V. W. Janssens, F. Joensen, S. Bordiga and K. P. Lillerud, *Angew. Chem., Int. Ed.*, 2012, **51**, 5810–5831.

5 C. Mei, P. Wen, Z. Liu, H. Liu, Y. Wang, W. Yang, Z. Xie, W. Hua and Z. Gao, *J. Catal.*, 2008, **258**, 243–249.
6 J. Liu, C. Zhang, Z. Shen, W. Hua, Y. Tang, W. Shen, Y. Yue and H. Xu, *Catal. Commun.*, 2009, **10**, 1506–1509.
7 J. C. Védrine, A. Auroux, P. Dejaifve, V. Ducarme, H. Hoser and S. Zhou, *J. Catal.*, 1982, **73**, 147–160.
8 A. Rahman, A. Adnot, G. Lemay, S. Kaliaguine and G. Jean, *Appl. Catal.*, 1989, **50**, 131–147.
9 S. M. Abubakar, D. M. Marcus, J. C. Lee, J. O. Ehresmann, C. Y. Chen, P. W. Kletnieks, D. R. Guenther, M. J. Hayman, M. Pavlova, J. B. Nicholas and J. F. Haw, *Langmuir*, 2006, **22**, 4846–4852.
10 P. Li, W. Zhang, X. Han and X. Bao, *Catal. Lett.*, 2010, **134**, 124–130.
11 K. H. Chandawar, S. B. Kulkarni and P. Ratnasamy, *Appl. Catal.*, 1982, **4**, 287–295.
12 J. A. Lercher and G. Rumplmayr, *Appl. Catal.*, 1986, **25**, 215–222.
13 F. Bleken, M. Bjørgen, L. Palumbo, S. Bordiga, S. Svelle, K.-P. Lillerud and U. Olsbye, *Top. Catal.*, 2009, **52**, 218–228.
14 G. Lischke, R. Eckelt, H. G. Jerschkewitz, B. Parlitz, E. Schreier, W. Storek, B. Zibrowius and G. Öhlmann, *J. Catal.*, 1991, **132**, 229–243.
15 J. Zhuang, D. Ma, G. Yang, Z. Yan, X. Liu, X. Liu, X. Han, X. Bao, P. Xie and Z. Liu, *J. Catal.*, 2004, **228**, 234–242.
16 G. Yang, J. Zhuang, Y. Wang, D. Zhou, M. Yang, X. Liu, X. Han and X. Bao, *J. Mol. Struct.*, 2005, **737**, 271–276.
17 T. Blasco, A. Corma and J. Martínez-Triguero, *J. Catal.*, 2006, **237**, 267–277.
18 G. Caeiro, P. Magnoux, J. M. Lopes, F. R. Ribeiro, S. M. C. Menezes, A. F. Costa and H. S. Cerqueira, *Appl. Catal., A*, 2006, **314**, 160–171.
19 M. Cardoso, D. Rosas and L. Lau, *Adsorption*, 2005, **11**, 577–580.
20 S. M. Cabral de Menezes, Y. L. Lam, K. Damodaran and M. Pruski, *Microporous Mesoporous Mater.*, 2006, **95**, 286–295.
21 G. Zhao, J. Teng, Z. Xie, W. Jin, W. Yang, Q. Chen and Y. Tang, *J. Catal.*, 2007, **248**, 29–37.
22 Y.-J. Lee, J. M. Kim, J. W. Bae, C.-H. Shin and K.-W. Jun, *Fuel*, 2009, **88**, 1915–1921.
23 Y.-J. Lee, Y.-W. Kim, N. Viswanadham, K.-W. Jun and J. W. Bae, *Appl. Catal., A*, 2010, **374**, 18–25.
24 D. Liu, W. C. Choi, C. W. Lee, N. Y. Kang, Y. J. Lee, C.-H. Shin and Y. K. Park, *Catal. Today*, 2011, **164**, 154–157.
25 M. Cardoso, D. Rosas and L. Lau, *Adsorption*, 2005, **11**, 577–580.
26 W. W. Kaeding and S. A. Butter, *J. Catal.*, 1980, **61**, 155–164.
27 M. Göhlich, W. Reschetilowski and S. Paasch, *Microporous Mesoporous Mater.*, 2011, **142**, 178–183.
28 A. Jentys, G. Rumplmayr and J. A. Lercher, *Appl. Catal.*, 1989, **53**, 299–312.
29 K. Damodaran, J. W. Wiench, S. M. Cabral de Menezes, Y. L. Lam, J. Trebosc, J. P. Amoureux and M. Pruski, *Microporous Mesoporous Mater.*, 2006, **95**, 296–305.
30 R. Lü, Z. Cao and S. Wang, *THEOCHEM*, 2008, **865**, 1–7.

31 S. L. Suib, A. M. Winiecki and A. Kostapapas, *Langmuir*, 1987, **3**, 483–488.

32 G. Sastre, D. W. Lewis and C. R. A. Catlow, *J. Phys. Chem.*, 1996, **100**, 6722–6730.

33 J. Klinowski, *Annu. Rev. Mater. Sci.*, 1988, **18**, 189–218.

34 M. Hunger, in *Catalytically Active Sites: Generation and Characterization*, ed. J. Čejka, A. Corma and S. Zones, Wiley-VCH, Weinheim, 2010, pp. 493–546.

35 G. L. Woolery, G. H. Kuehl, H. C. Timken, A. W. Chester and J. C. Vartuli, *Zeolites*, 1997, **19**, 288–296.

36 J. A. van Bokhoven, D. C. Koningsberger, P. Kunkeler, H. van Bekkum and A. P. M. Kentgens, *J. Am. Chem. Soc.*, 2000, **122**, 12842–12847.

37 N.-Y. Topsøe, K. Pedersen and E. G. Derouane, *J. Catal.*, 1981, **70**, 41–52.

38 X. Lin, Y. Fan, Z. Liu, G. Shi, H. Liu and X. Bao, *Catal. Today*, 2007, **125**, 185–191.

39 J.-P. Gilson, G. C. Edwards, A. W. Peters, K. Rajagopalan, R. F. Wormsbecher, T. G. Roberie and M. P. Shatlock, *J. Chem. Soc., Chem. Commun.*, 1987, 91–93.

40 V. L. Zholobenko, L. M. Kustov, V. Y. Borovkov and V. B. Kazansky, *Zeolites*, 1988, **8**, 175–178.

41 N. Xue, R. Olindo and J. A. Lercher, *J. Phys. Chem. C*, 2010, **114**, 15763–15770.

42 J. Caro, M. Bülow, M. Derewinski, J. Haber, M. Hunger, J. Kärger, H. Pfeifer, W. Storek and B. Zibrowius, *J. Catal.*, 1990, **124**, 367–375.

43 K. Eichele and R. E. Wasylishen, *J. Phys. Chem.*, 1994, **98**, 3108–3113.

44 L. R. Aramburo, E. de Smit, B. Arstad, M. M. van Schooneveld, L. Sommer, A. Juhin, T. Yokosawa, H. W. Zandbergen, U. Olsbye, F. M. F. de Groot and B. M. Weckhuysen, *Angew. Chem., Int. Ed.*, 2012, **51**, 3616–3619.

45 J. A. van Bokhoven, D. C. Koningsberger, P. Kunkeler and H. van Bekkum, *J. Catal.*, 2002, **211**, 540–547.

46 A. Omegna, R. Prins and J. A. van Bokhoven, *J. Phys. Chem. B*, 2005, **109**, 9280–9283.

47 J. A. van Bokhoven, A. M. J. van der Eerden and D. C. Koningsberger, *J. Am. Chem. Soc.*, 2003, **125**, 7435–7442.

48 E. Loeffler, U. Lohse, C. Peuker, G. Oehlmann, L. M. Kustov, V. L. Zholobenko and V. B. Kazansky, *Zeolites*, 1990, **10**, 266–271.

49 O. Lisboa, M. Sanchez and F. Ruette, *J. Mol. Catal. A: Chem.*, 2008, **294**, 93–101.

50 S. Malola, S. Svelle, F. L. Bleken and O. Swang, *Angew. Chem., Int. Ed.*, 2012, **51**, 652–655.

51 T. Fjermestad, S. Svelle and O. Swang, *J. Phys. Chem. C*, 2013, **117**, 13442–13451.

52 I. Lukes, M. Borbaruah and L. D. Quin, *J. Am. Chem. Soc.*, 1994, **116**, 1737–1741.

53 M. J. D. Low and P. Ramamurthy, *J. Phys. Chem.*, 1968, **72**, 3161–3167.

54 E. Bourgeat-Lami, P. Massiani, F. Di Renzo, P. Espiau, F. Fajula and T. Des Courières, *Appl. Catal.*, 1991, **72**, 139–152.

55 T.-H. Chen, B. H. Wouters and P. J. Grobet, *J. Phys. Chem. B*, 1999, **103**, 6179–6184.

56 A. Stanislaus, M. Absi-Halabi and K. Al-Doloma, *Appl. Catal.*, 1988, **39**, 239–253.

57 E. C. de Oliveira Lima, J. M. Moita Neto, F. Y. Fujiwara and F. Galembeck, *J. Colloid Interface Sci.*, 1995, **176**, 388–396.

58 D. Massiot, F. Fayon, M. Capron, I. King, S. Le Calvé, B. Alonso, J.-O. Durand, B. Bujoli, Z. Gan and G. Hoatson, *Magn. Reson. Chem.*, 2002, **40**, 70–76.

59 G. Seo and R. Ryoo, *J. Catal.*, 1990, **124**, 224–230.

60 H. E. van der Bij, L. R. Aramburo, B. Arstad, J. J. Dynes, J. Wang and B. M. Weckhuysen, *ChemPhysChem*, 2013, DOI: 10.1002/cphc.201300910.

This journal is © the Owner Societies 2014

Phys. Chem. Chem. Phys., 2014, **16**, 9892–9903 | 9903